remote sensing

MDPI

Article

Effect of ENSO on the Ozone Valley over the Tibetan Plateau Based on the WACCM4 Model

Yongchi Li [1], Feng Xu [1], Lingfeng Wan [2], Peng Chen [1], Dong Guo [3,4], Shujie Chang [1,5,*] and Chen Yang [3,4]

1 College of Ocean and Meteorology, South China Sea Institute of Marine Meteorology, Key Laboratory of Climate, Resources and Environment in Continental Shelf Sea and Deep Sea of Department of Education of Guangdong Province, Laboratory for Coastal Ocean Variation and Disaster Prediction, Guangdong Ocean University, Zhanjiang 524088, China
2 Frontier Science Center for Deep Ocean Multispheres and Earth System (DOMES), Physical Oceanography Laboratory (POL), Institute for Advanced Ocean Study (IAOS), Ocean University of China, Qingdao 266100, China
3 Key Laboratory of Meteorological Disaster, Ministry of Education (KLME), Joint International Research Laboratory of Climate and Environment Change (ILCEC), Collaborative Innovation Center on Forecast and Evaluation of Meteorological Disasters, Nanjing University of Information Science and Technology, Nanjing 210044, China
4 Reading Academy, Nanjing University of Information Science and Technology, Nanjing 210044, China
5 Key Laboratory of Space Ocean Remote Sensing and Application, Ministry of Natural Resources, Beijing 100081, China
* Correspondence: changsj@gdou.edu.cn; Tel.: +86-134-13617846

Abstract: El Niño-Southern Oscillation (ENSO) is the most significant global ocean–atmosphere coupled signal in the tropical Pacific Ocean, and it can affect the stratosphere. However, the ENSO-related dynamical processes that influence the ozone valley during summer are still not well understood and are under-investigated. In this study, we used the ERA5 and MERRA-2 reanalysis data from 1979 to 2021 combined with numerical simulations to analyze the mechanisms through which ENSO affects the ozone valley over the Tibetan Plateau in the upper troposphere and the lower stratosphere (UTLS) in summer. The results showed that the two cores of the ozone valley in UTLS were more evident in the summer following La Niña than in the summer following El Niño. At low latitudes, negative O_3 anomalies in UTLS were observed in the summer following El Niño and positive O_3 anomalies were observed in the summer following La Niña. At middle latitudes, negative O_3 anomalies in UTLS were found near 60°E in the summer following El Niño, while negative anomalies were found at 40°E and 120°E in the summer following La Niña. The analysis of the flow and vorticity fields suggested that the field anomalies can cause vertical motion, which in turn leads to the mixing of different ozone concentrations and affects the ozone valley in UTLS over the Tibetan Plateau. In particular, the warming of the Indian Ocean sea-surface temperature (SST) in the summer following El Niño enhances the South Asian High (SAH) through two-stage thermal adaptation, leading to ozone anomalies at low latitudes in the ozone-valley region. These conclusions were verified by a simulation using the WACCM4 model, the results of which were consistent with the original observations.

Keywords: ENSO; ozone valley; Tibetan Plateau; WACCM

check for updates

Citation: Li, Y.; Xu, F.; Wan, L.; Chen, P.; Guo, D.; Chang, S.; Yang, C. Effect of ENSO on the Ozone Valley over the Tibetan Plateau Based on the WACCM4 Model. *Remote Sens.* **2023**, *15*, 525. https://doi.org/10.3390/rs15020525

Academic Editor: Manuel Antón

Received: 22 November 2022
Revised: 13 January 2023
Accepted: 14 January 2023
Published: 16 January 2023

1. Introduction

The ozone is one of the most important trace components in the atmosphere and can block the ultraviolet radiation from the sun due to its strong absorption of solar ultraviolet radiation (0.2~0.29 μm). Furthermore, the ozone in the stratosphere absorbs solar ultraviolet radiation to warm the stratosphere atmosphere as the main heat source and to change the thermal and dynamic structure of the stratosphere [1–7], which plays an extremely important role in the normal survival and reproduction of life on Earth. The ozone is mainly distributed in the stratosphere atmosphere in the 10–50 km range, with the number-density maxima between 20 and 30 km. Only 10% of the ozone is in the troposphere. With the continuous advancement of observation technology [8–10], it is found that the stratospheric and tropospheric ozone are connected by the upper troposphere and lower stratosphere (UTLS) areas, which is important for material exchange [11–15]; changes in ozone concentrations in this region can affect the global climate [16–18]. Global warming is a widely accepted view nowadays, and the climate change it causes is of great importance [19,20]. The ozone layer, due to its energy-absorption and heating characteristics, determines the temperature field and atmospheric circulation of the stratosphere and plays a very important role in establishing the atmospheric vertical temperature structure and atmospheric-radiation balance within the global-warming framework. Therefore, the study of the total atmospheric ozone has long been a major research focus in Earth sciences.

El Niño–Southern Oscillation (ENSO) is the most significant global-scale ocean–atmosphere coupled signal in the tropical Pacific Ocean. As a typical tropical Pacific air–sea system that affects large-scale circulation anomalies, ENSO influences not only the tropical Pacific climate anomalies but also the atmospheric remote response to tropical and global climate anomalies [21]. As the strongest interannual climate-anomaly signal, ENSO can affect the stratosphere [22] by influencing the stratospheric ozone with different time lags in different regions [23–26]. The ENSO mainly affects the tropical stratospheric ozone by changing the advection of the tropical upwellings. At mid-to-high latitudes, advection changes can modify the residual circulation subsidence, and the occurrence of horizontal mixing is associated with Rossby-wave-breaking and polar-vortex anomalies [27–31].

The ozone valley over the Tibetan Plateau is a phenomenon of ozone loss that forms a low-value center in the UTLS over the Tibetan Plateau. Xiuji Zhou et al. [32] used the total ozone mapping spectrometer (TOMS) data from 1979 to 1991 to calculate the spatial and temporal distribution of the average monthly ozone over 13 years, recognizing the ozone loss over the Tibetan Plateau in summer (June to September), i.e., the ozone valley over the Tibetan Plateau. Furthermore, micro-ozone holes or very-low-value ozone events also occur over the Tibetan Plateau in winter [33]. Guo Dong et al. [34] studied the relationship between the strongest centers of the ozone valley in the UTLS and the South Asian high (SAH) by using data from the stratospheric aerosol and gas experiment (SAGE) satellite data. They found a low-value center in the stratosphere and confirmed the two-core structure of the ozone valley for the first time through microwave limb sounder (MLS) satellite data. Most researchers believe that the formation of the ozone valley over the Qinghai–Tibetan Plateau is mainly driven by changes in atmospheric dynamics rather than chemistry [34–38].

The summer ozone over the Tibetan Plateau is greatly affected by tropical processes [39]. Therefore, ENSO, as a strong tropical interannual signal, is expected to have a strong connection with the ozone valley over the Tibetan Plateau. Previous studies showed that ENSO can shock the ozone over the Qinghai–Tibetan Plateau, and the impact can last for about a year [40–43]. In addition, the first main mode of EOF decomposition of the total-column-ozone-latitude deviation in the UTLS area of the Qinghai–Tibetan Plateau is closely related to ENSO [44].

Although initial progress has been made in investigating the impact of ENSO on the ozone valley over the Tibetan Plateau, validation through numerical-simulation experiments in these studies is still lacking. The Whole Atmosphere Community Climate Model (WACCM), supported by the National Center for Atmospheric Research (NCAR) climate model, is a relatively sound climate model describing atmospheric physics and chemical processes. The WACCM is widely applicable to stratosphere processes and can give good simulation results for ozone changes [45,46]. Version 4 of the WACCM, WACCM4, can simulate ENSO signals in the atmosphere [47]. To fill in the gap in numerical-simulation experiments in the study of ENSO affecting the ozone valley over the Tibetan Plateau, this paper focuses on the connection and physical mechanism by using WACCM4 to simulate the ozone in the context of ENSO over the Tibetan Plateau.

The components of this paper are as follows. Section 2 briefly presents the data and the methods. Section 3 explores the effects of ENSO on the ozone valley of the Tibetan Plateau. Section 4 explores the possible impact mechanism of ENSO in the ozone valley through an analysis. The results were verified by the numerical-simulation experiments reported in Section 5. A discussion and conclusions follow in Section 6.

2. Data and Methods

2.1. Observational Data

This paper uses ozone mass mixing ratio, horizontal wind, vertical velocity, air pressure, potential height, and sea-surface temperature (SST) data from ERA5 with a horizontal resolution of $0.25° \times 0.25°$ and vertical stratification from 1000 hPa to 1 hPa supported by the European Center for Medium-Range Weather Forecasts (ECMWF) (https://www.ecmwf.int/en/forecasts/datasets/reanalysis-datasets/era5, accessed on 4 December 2021). The ozone mass mixing ratio used was from MERRA-2 (Modern-Era Retrospective Analysis for Research and Applications, version 2) satellite data from the National Aeronautics and Space Administration (NASA) with a horizontal resolution of $0.625° \times 0.5°$, and the vertical grid of the ozone mass mixing ratio ranged from 1000 hPa to 0.1 hPa. The Nino 3.4 index data used were from the Climate Prediction Center (CPC) (https://psl.noaa.gov/data/correlation/nina34.anom.data, accessed on 4 December 2021). The summer (June–August) data from 1979 to 2021 were selected for this study.

2.2. WACCM 4 Numerical-Simulation Experiment

The WACCM4 has two operational options. The 'full interactive chemistry' turns on the chemical-radio-dynamic feedback process, while the other, 'greenhouse gas', turns it off [48]. The chemical-radio-dynamic feedback of the WACCM4 model refers to the interconnection of the dynamical module, the chemical module, and the radiation-parameterization scheme in the model operation, which better reflects the coupling process of dynamics, chemistry, and radiation in the atmosphere. The dynamical module ensures the conservation of atmospheric composition and energy, the chemical module takes into account the microscopic processes of heat and ions generated by chemical reactions, and the radiation-parameterization scheme takes into account the effects of short and long waves. The coordinates in the vertical direction of the WACCM4 model have 66 layers, extending from the ground to the pressure level at 4.5×10^{-6} hPa (~about 145 km height). The vertical resolution was 1.1–1.4 km in the top tropical troposphere (TTL) area and the lower stratosphere (<30 km). All experiments in this study were performed with a horizontal resolution of $1.9° \times 2.5°$ using a full chemical-interaction process.

2.3. Methods

The low-value center of latitudinal deviation of the total column ozone (TCO*) was used to characterize the ozone valley. The definition of TCO* and the calculation method of the height integration were described by Chang [44]: $TCO^* = O_3 - \overline{O_3}$, where O_3 is the total column ozone in the selected height range, and $\overline{O_3}$ is the zonal average of total column ozone in the selected height range. In this paper, we use the height range of the UTLS (about 50–300 hPa).

In this paper, the El Niño (La Niña) event is defined by the five-month moving average Nino 3.4 index > 0.5 °C (<0.5 °C). A total of 43 years of El Niño and La Niña were selected by the Nino 3.4 index standardized-time-series map (Figure 1). The El Niño years are 1982, 1983, 1987, 1992, 1994, 1997, 1998, 2002, 2004, 2009, 2015, 2016, and 2019. The La Niña years are 1980, 1981, 1984, 1985, 1988, 1989, 1990, 1999, 2000, 2007, 2008, 2010, 2011, 2020, and 2021. In addition, since the years with a weak or a less strong phenomenon were excluded, only the typical El Niño and La Niña years were selected.

We also simulated the ozone, wind, and relative vorticity in ENSO years to investigate the influence of ENSO on the ozone valley over the Tibetan Plateau and its mechanism.

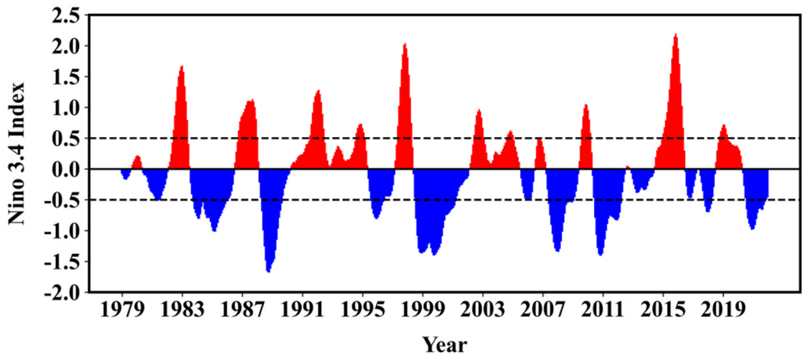

Figure 1. Time series of the Nino 3.4 index in 1979−2021.

3. Connection between ENSO and the Ozone Valley over the Tibetan Plateau

3.1. Spatiotemporal-Distribution Characteristics of the Ozone Valley over the Tibetan Plateau

The ozone valley over the Tibetan Plateau is mainly distributed in the UTLS [34]. Figure 2 gives an intuitive understanding of the ozone valley over the Tibetan Plateau in the UTLS and shows the spatial distribution of the time-averaged TCO* from 1979 to 2021.

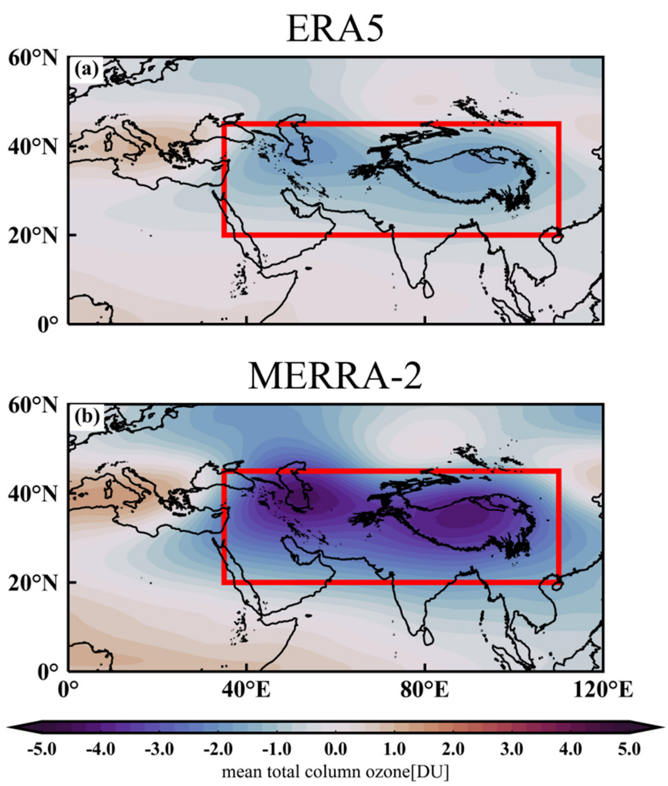

Figure 2. Climatological TCO* in summer (**a**) ERA−5 (**b**) MERRA−2 (unit: DU).

The average-distribution map of TCO* obtained from the two satellite reanalysis datasets shows the ozone valley over the Tibetan Plateau, with the ozone-loss center mainly located at 35°–110°E and 30°–45°N (in the red box of Figure 2). On the distribution map obtained using the ERA5 data, the lowest TCO* in the center of the ozone valley is about −1.8 DU (Figure 2a). On the distribution map obtained using the MERRA-2 ozone-mass-mixing-ratio data, the lowest TCO* in the center of the ozone valley reaches −4.3 DU, and the surrounding areas reach −3.4 DU to −4.0 DU (Figure 2b). Although the values are different, both maps show the same average latitude deviation of negative ozone over the Tibetan Plateau, reflecting the total ozone loss over the Tibetan Plateau and the low-ozone-value center.

3.2. Relationship of ENSO with the Ozone over the Tibetan Plateau

To understand the connection between ENSO and the ozone over the Tibetan Plateau, the correlation coefficient between the Nino 3.4 index and the TCO* in the main UTLS region (35°–110°E, 30°–45°N over the Tibetan Plateau) was calculated. Chang et al. illustrated the relationship between the Nino 3.4 index and the TCO* index (TCOI) of the ozone in the UTLS of the Tibetan Plateau, indicating that the Nino 3.4 index has a 6-month lead with respect to TCO* [49]. Thus, ENSO is ahead of the ozone in the UTLS over the Tibetan Plateau and is in the same phase.

According to this hypothesis, we expected ENSO to affect the ozone in the UTLS over the Tibetan Plateau in the following summer. To verify this, we analyzed the average distribution of TCO* in UTLS in the year following El Niño and La Niña.

As shown in Figure 3, both the TCO* distribution maps obtained using the ERA5 data or the MERRA-2 data show the TCO* low-value center over the Tibetan Plateau in the UTLS with a two-core-structure ozone valley in the summer following a typical El Niño. Figure 3a shows that the low TCO* center reached −1.8 DU, and the lowest negative TCO* latitudinal deviation in Figure 3b reached −4.2 DU. In the following summer, when a typical La Niña occurred, the TCO* depletion or the influencing area strengthened. Figure 3c shows that the low TCO* area extended to the west and even rose north from the Caspian Sea to connect with the Arctic Circle. Figure 3d exhibits a more obvious TCO* depletion of up to −4.0 DU and a larger low-value area compared to Figure 3c.

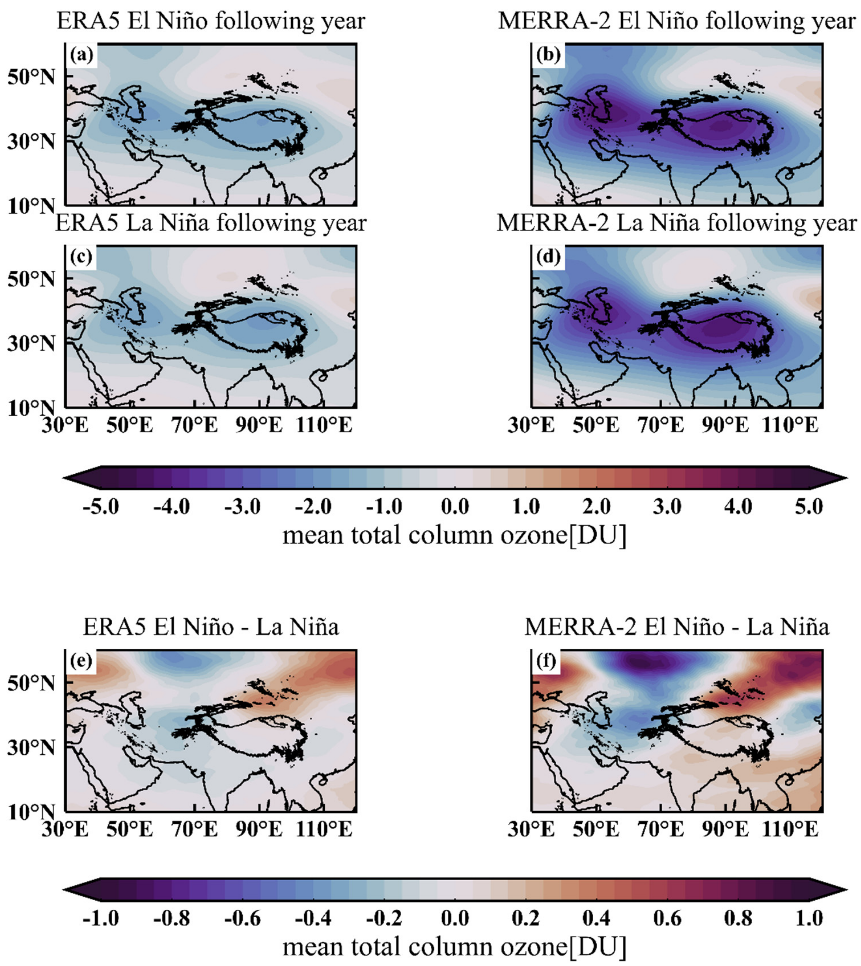

Figure 3. Composite TCO* in the summer following El Niño and La Niña (unit: DU): (**a**) El Niño based on ERA5, (**b**) El Niño based on MERRA−2, (**c**) La Niña based on ERA5, (**d**) La Niña based on MERRA−2, (**e**) the difference between El Niño and La Niña based on ERA5, (**f**) the difference between El Niño and La Niña based on MERRA−2.

Figure 3e,f shows the results obtained in the summer following El Niño minus the summer following La Niña, which shows the difference in the distribution of the TCO* in the two phases of ENSO. The two datasets showed a consistent distribution, with positive values mainly in the Caspian Sea and its northwestern part, the Tibetan Plateau and its northeastern part, located near the two cores of the ozone valley, reaching maxima of 1 DU (ERA5) and 1.9 DU (MERRA-2). The negative values were mainly located in the middle of the two positive areas, reaching −0.7 DU (ERA5) and −1.5 DU (MERRA-2). These caused the ozone valley to be more pronounced in the summer following La Niña compared to El Niño.

Overall, the low TCO* distribution in the UTLS in the year following La Niña was wider with more pronounced TCO* depletion than that in the year following El Niño.

To further reveal the impact of ENSO on the ozone over the Tibetan Plateau in the UTLS, we started with anomaly distributions to find the relationship between ENSO and the total O_3.

The O_3-anomaly distributions in the UTLS in the summers following El Niño and La Niña are shown in Figure 4. The results based on ERA5 and MERRA-2 were generally consistent. In the south of the ozone-valley region, the summer O_3 anomalies following El Niño and La Niña were opposite to each other. The O_3 anomalies were around −0.2 DU to −0.4 DU in the summer following El Niño (Figure 5a) but were mostly positive, around 0.15 DU, in the summer following La Niña (Figure 5b). Due to the asymmetry of ENSO, the distribution of its effects did not correspond exactly. The range of negative O_3 anomalies in the summer following El Niño was larger than the range of positive anomalies in the summer following La Niña, with one positive anomaly in the north of the Tibetan Plateau. In addition, in the northern region, the summer following El Niño and La Niña showed mostly negative anomalies, located near 60°E following El Niño and near 40°E and 120°E following La Niña. All these results suggest that El Niño leads to a decrease in O_3 in most of the ozone-valley area in the following summer, while La Niña causes an increase in O_3 in the south but a decrease in O_3 in the north of the ozone valley.

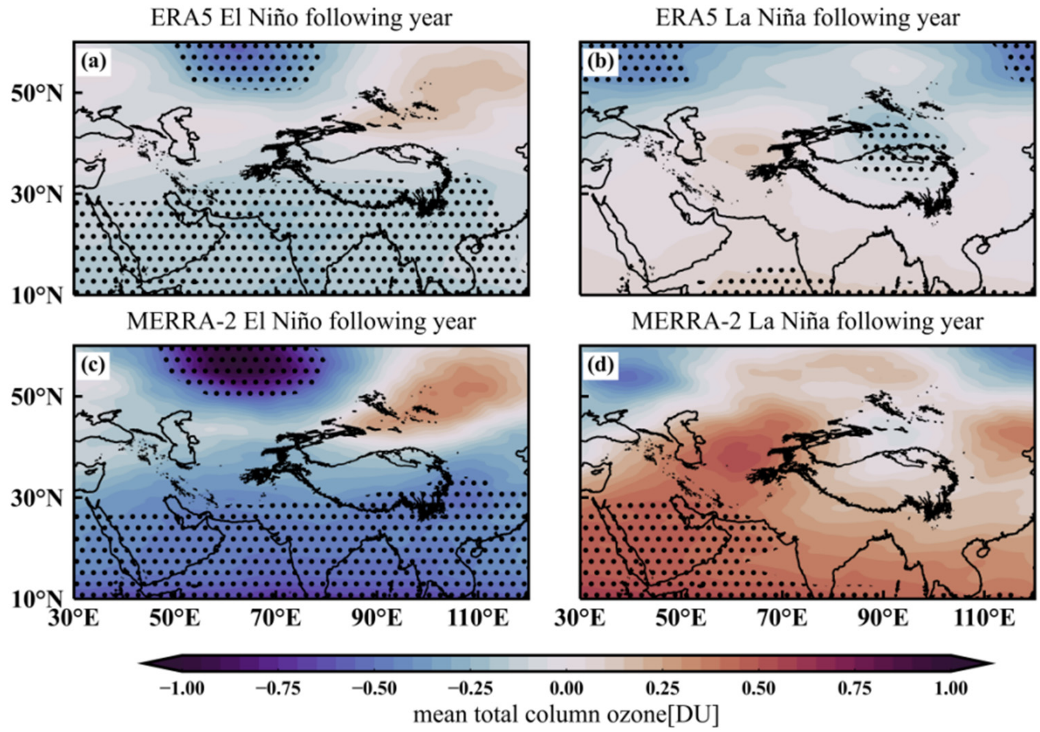

Figure 4. Composite O_3 anomalies in the summers following El Niño and La Niña (unit: DU). (**a**) El Niño based on ERA5, (**b**) La Niña based on ERA5, (**c**) El Niño based on MERRA-2, (**d**) La Niña based on MERRA-2. The black-dotted regions are statistically significant at the 95% confidence level (*t*-test).

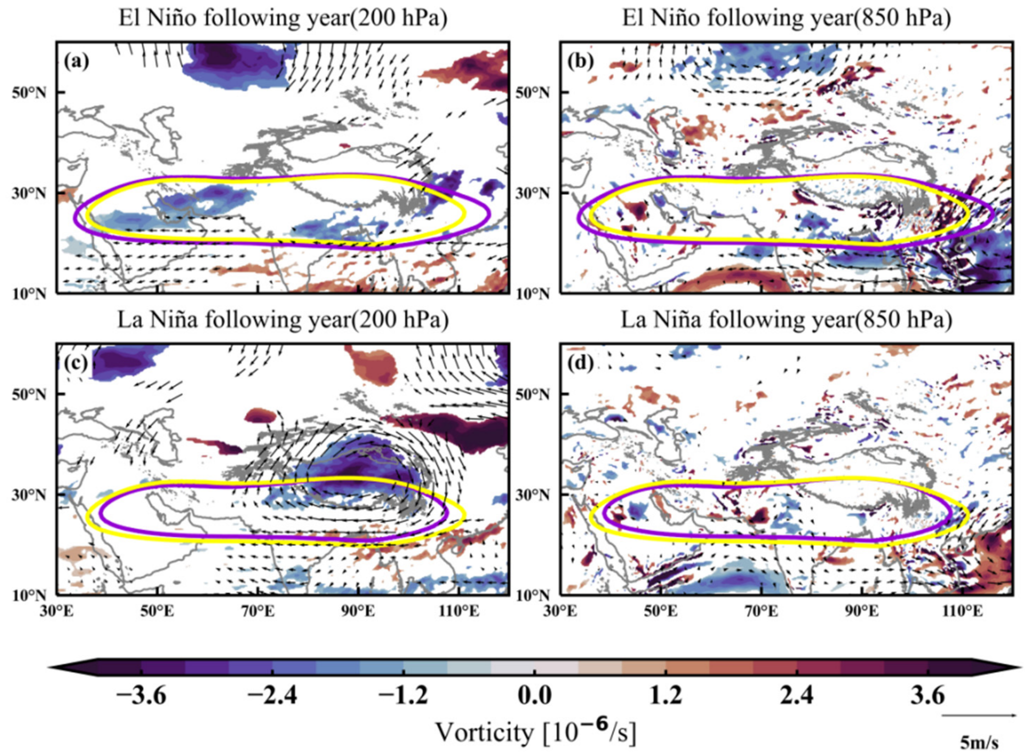

Figure 5. Composite wind anomalies at 850 hPa and 200 hPa (arrows, unit: m/s), with the SAH region averaged (solid yellow lines, 12,520 gpm, geopotential height isolines), and relative-vorticity anomalies (shading, unit: 10^{-6}/s) in the summers following El Niño and La Niña. (**a**) El Niño at 200 hPa, (**b**) El Niño at 850 hPa, (**c**) La Niña at 200 hPa, (**d**) La Niña at 850 hPa. The solid purple lines indicate the climatological location of the SAH region. The results above the 95% confidence level (*t*-test) are indicated.

In conclusion, the El Niño climate plays a crucial role in ozone depletion and the formation of ozone low-value centers in the study area, especially in the Tibetan Plateau. The following section explores how ENSO affects the ozone over the Tibetan Plateau in the UTLS.

4. Analysis of the Effect of ENSO on the Ozone Valley over the Tibetan Plateau

The dynamics are important factors affecting the ozone valley over the Tibetan Plateau in the UTLS, and we can study the effects of ENSO by analyzing the circulation field.

Figure 5 shows the upper- and lower-atmosphere circulation and SST anomalies in the summers following El Niño or La Niña. The level of 200 hPa is more representative of the UTLS. Figure 5a shows scattered negative vorticity in the south of the ozone valley in the 200-hectopascal altitude layer, representing a weak anticyclonic circulation combined with the wind field in the summer following El Niño. This anticyclonic circulation can pump the low-concentration ozone to a higher level, reducing the ozone concentration in the UTLS, which also corresponds to the negative anomalies of O_3 in the south in Figure 4. In the north of the ozone-valley region, at heights of both 200 hPa and 850 hPa, an anticyclonic circulation to the west and a cyclonic circulation to the east are observed.

In the summer following La Niña, cyclonic circulation in the west and anticyclonic circulation in the east of the 200-hectopascal ozone valley occurred, as shown in Figure 5c. This pumped down the higher ozone concentration in the west and pumped up the low ozone concentration in the east, corresponding to the opposite O_3 anomalies in the east and west in Figure 4b.

Previous studies showed that abnormal SAH pressure is one of the important factors that affect the ozone [34,50]. Figure 5 shows that the SAH position corresponded to the anticyclonic circulation in the southern part of the ozone-valley region, and that the SAH was enhanced in the summer following El Niño. This enhancement was caused by the positive sea-surface-temperature anomalies (SSTA) in the Indian Ocean in the following summer (Figure 6), through the second level of thermal adaptation in the two-stage thermal adaptation in the atmosphere [51]. The theory of the two-stage thermal adaptation proposes that the sensible heat generated by the warm SSTA in the Indian Ocean makes the eastern side of the Indian Ocean produce southerly winds, which bring the abundant water vapor from the ocean to the land and produce rainfall. The latent heating, which is located in the mid-troposphere, decreases with increasing height, resulting in anticyclonic anomalies in the upper layers and the strengthening of the SAH. This further leads to the strengthening of the westward extension of the West Pacific subtropical high and the abnormal enhancement of the SAH, corresponding to the anticyclone-circulation anomalies in the lower layer in the northwest-Pacific region in Figure 5b and the anticyclone-circulation anomalies in southern Asia in Figure 5a.

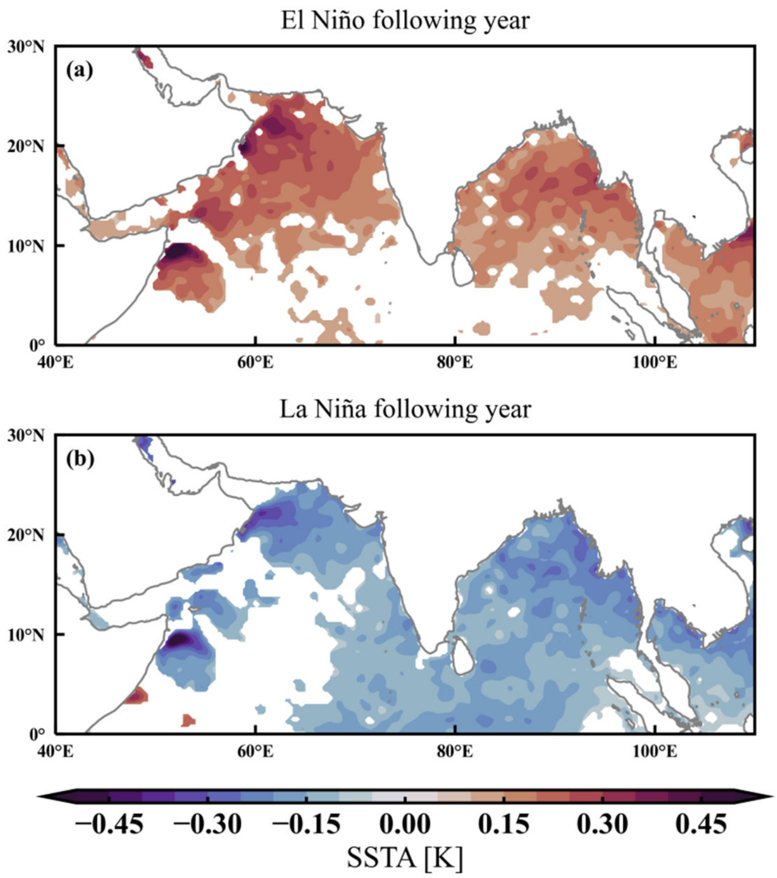

Figure 6. Indian Ocean SSTA in the summer following El Niño and La Niña (shading, unit: K) (**a**) El Niño based on ERA5, (**b**) La Niña based on ERA5. The results above the 95% confidence level (*t*-test) are indicated.

5. Simulated ENSO Effects on the Ozone over the Tibetan Plateau

The relationship between and influence mechanism underlying ENSO and the ozone in the UTLS over the Tibetan Plateau were discussed in the previous sections. The simulation results using the WACCM4 model are illustrated here to further strengthen our hypothesis.

For the external forcing of the WACCM4-model experiment, the SSTA time series from Figure 1 were used. The composite SSTAs are shown by the thick red lines in Figure 7.

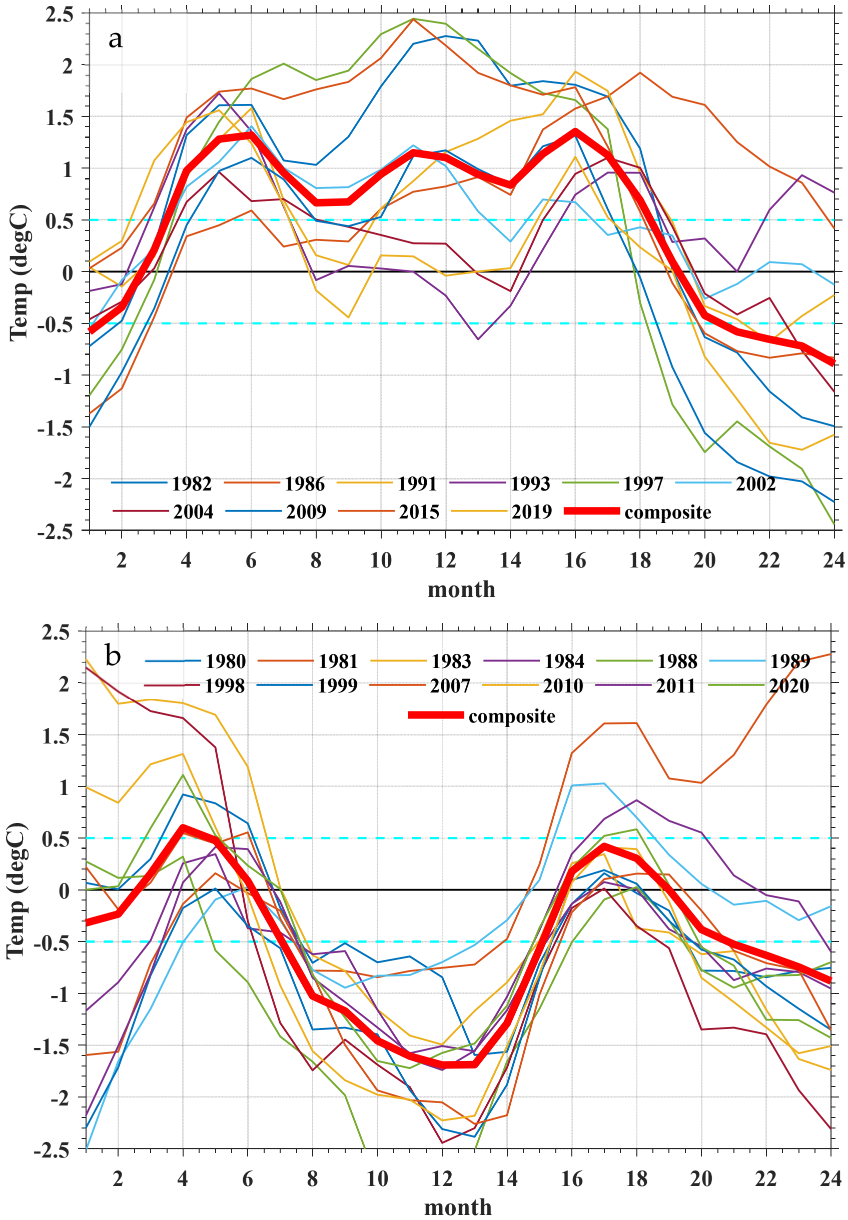

Figure 7. The SSTAs in the 5°S−5°N, 190°E−240°E region from the selected ENSO events. (**a**) El Niño, (**b**) La Niña. Thin lines represent the ENSO events, and thick lines represent the composite SSTA obtained by averaging the SSTAs.

This experiment added the El Niño (La Niña) event SSTAs in the 5°S–5°N region to simulate the response of the UTLS ozone to ENSO events for the 1955–2005 period (Table 1). For model balance, the first 5 years with normal SSTAs were used as the spin-up time. For the following 2 years, the composite SSTA of El Niño (La Niña) in Figure 7 were used to impose forcing. The duration of the composite SSTA of El Niño (La Niña) in Figure 7 is two years, that is, 24 months. The months in which the SSTAs were less (or more) than 0.5 °C were replaced with the normal SSTAs, after which the modified SSTAs were used to impose forcing. The SSTA forcing of a 2-year El Niño (La Niña) was applied every 3 years, and the normal SSTAs were used in the remaining years. For comparison, this study also simulated the SSTAs of normal years by adding the last 20 years as the climate state in normal years for 33 consecutive years.

Table 1. Simulation experiment design.

Trial	Simulation Period	Simulation Process
E1	1955–2005	The SSTA force was applied at 5°S–5°N, 190°E–120°W. The normal-year SSTAs are given for the first 5 years as the spin-up. Next, the SSTA of the composite El Niño events was added for every five years. For the composite El Niño covering 5 years, we used the monthly SSTAs to predict the months with SSTA > 0.5 °C (<0.5 °C), and the monthly SSTAs for other months were synthesized in the normal years for the first 2 years. For the last 3 years, normal SSTA forcing was used. A total of nine observations of the composite El Niño events were added to the SSTA.
E2	1955–2005	Similar to E1, with the addition of the observed composite SSTA of La Niña events.

Figure 8 shows the distribution of the O_3 anomalies in the UTLS for the conditions in the summers following El Niño and La Niña. The O_3 anomalies showed a reverse change in the summers following El Niño and La Niña at low latitudes. They were negative, around −0.3 DU, following El Niño and positive, around 0.3 DU–0.44 DU, following La Niña. At middle latitudes, there were significant positive anomalies in the range of 90°E–120°E and insignificant negative anomalies in the range of 50°E–90°E in the summer following El Niño. Negative anomalies were present in the range of 30°E–50°E and 70°E–100°E in the summer following La Niña. The simulation results and the observed results (Figure 4) were in good agreement at low latitudes, with negative anomalies in the summer following El Niño and positive anomalies in the summer following La Niña. At middle latitudes, there were other signals in the real atmosphere in addition to ENSO, and the observed results deviated from the simulation results, reflecting the influence of ENSO on O_3. The comparison shows that the negative anomalies were roughly in the range of 40°E–80°E and that the positive anomalies are in the range of 80°E–120°E at middle latitudes, and the positive anomalies were more significant in the simulation results. By contrast, the two simulated negative-anomaly regions at middle latitudes in the summer following La Niña will have been more westward than those that were observed.

Figure 9 shows the simulated distribution of the horizontal winds and relative-vorticity anomalies at 200 hPa and 850 hPa in the summers following El Niño and La Niña. In the summer following El Niño, the upper-atmosphere circulation was characterized by anticyclonic circulation with negative-vorticity anomalies at low latitudes and in the northern ozone valley, and cyclonic circulation with positive-vorticity anomalies in the northeast of the Tibetan Plateau. In the summer following La Niña, strong cyclonic-circulation anomalies were present between the Iranian plateau and the Tibetan Plateau for the upper-atmosphere circulation, while anticyclonic circulation occurred over the Tibetan Plateau. The lower-atmosphere circulation was characterized by anticyclonic-circulation anomalies at low latitudes. The circulation-anomaly and vorticity-anomaly regions correspond to the O_3-anomaly region in Figure 8. These circulation dynamics directly caused the ozone changes. The simulated results roughly agreed with the observations in terms of distribution. In the summer following El Niño, anticyclonic-circulation anomalies and negative-vorticity anomalies in the upper level were present at low latitudes and near 70°E at middle latitudes, and cyclonic-circulation anomalies were present in the northwest of the Tibetan Plateau. For the summer following La Niña, a cyclonic-circulation anomaly and an anticyclonic-circulation anomaly in the upper level near 30°N corresponded well with the observations.

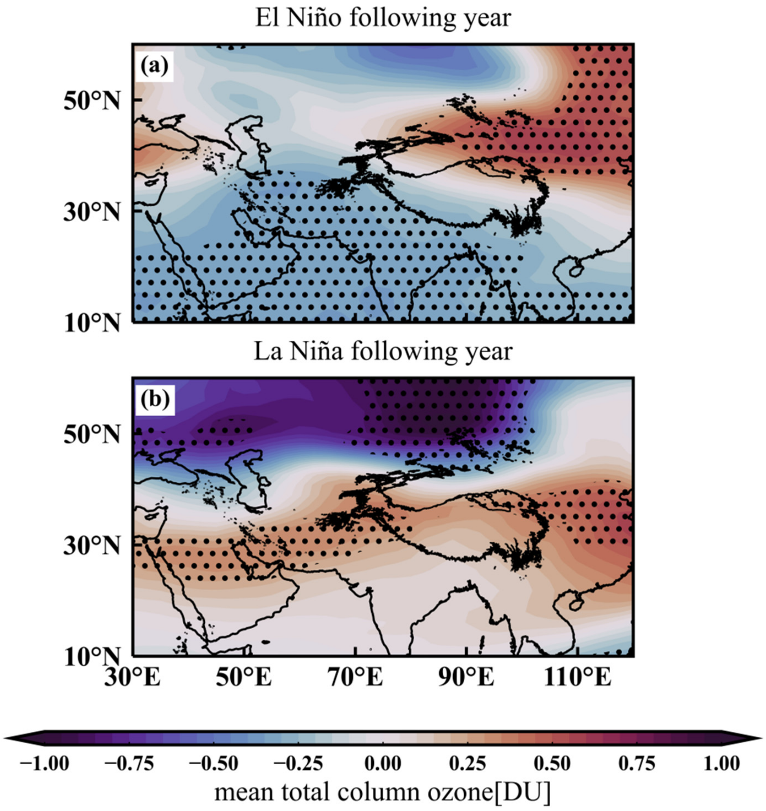

Figure 8. Simulation results of composite O_3 anomalies in the summers following El Niño and La Niña (unit: DU). (**a**) El Niño, (**b**) La Niña. The black-dotted regions are statistically significant at the 95% confidence level (*t*-test).

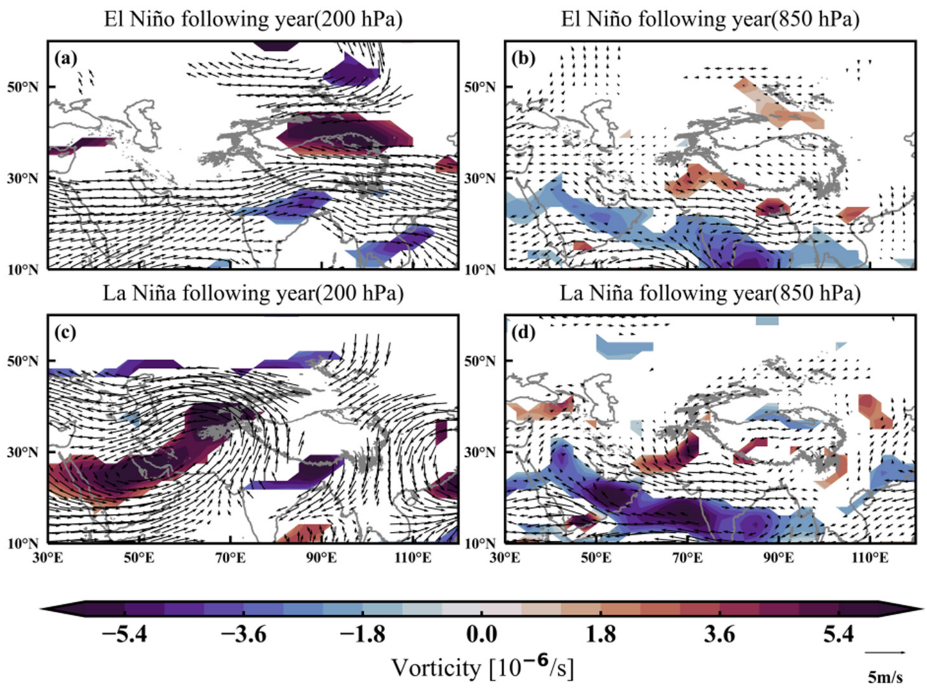

Figure 9. Simulation results of composite wind anomalies at 850 hPa and 200 hPa (arrows, unit: m/s), with the SAH region averaged (solid yellow lines, 12,520 gpm, geopotential height isolines), and relative-vorticity anomalies (shading, unit: 10^{-6}/s) in the summers following El Niño and La Niña. (**a**) El Niño at 200 hPa, (**b**) El Niño at 850 hPa, (**c**) La Niña at 200 hPa, (**d**) La Niña at 850 hPa. The results above the 95% confidence level (*t*-test) are indicated.

Overall, the simulation results were consistent with observations. The ozone and circulation simulations at low latitudes were more accurate because they revealed the negative anomalies in the summer following El Niño and the positive anomalies in the summer following La Niña. The simulation results for the O_3 at different latitudes also showed similar distributions, but at high latitudes some differences were noted due to other signal influences in addition to ENSO.

6. Conclusions and Discussion

This study used the ozone-mixing ratios of ERA5 and MERRA-2 in the summers of 43 years (1979–2021) to investigate the ozone over the Tibetan Plateau in the UTLS by analyzing the TCO*- and O_3-anomaly distributions. Based on the comparative analysis of the spatial- and temporal-distribution and intensity variations in the ozone in the summers following El Niño and La Niña, and combined with the SAH, we discussed the average SSTA field and wind field and the mechanism of ENSO's influence on the ozone valley over the Tibetan Plateau. Our hypothesis was further verified through model simulations. We can draw the following conclusions:

(1) The two cores of the ozone valley in the UTLS in the summer following La Niña are more obvious than those in the summer following El Niño. At low latitudes, negative O_3 anomalies in the UTLS were observed in the summer following El Niño, and positive O_3 anomalies were observed in the summer following La Niña. At middle latitudes, a negative O_3 anomaly was present in the UTLS near 60°E in the summer following El Niño, and negative anomalies at 40°E and 120°E occurred in the summer following La Niña.

(2) The analysis of the flow and vorticity fields suggested that the anomalies in these fields cause vertical motion, which in turn leads to the mixing of different concentrations of ozone and affects the ozone valley in the UTLS over the Tibetan Plateau. Anticyclonic (or cyclonic)-circulation anomalies transport low (or high) concentrations of ozone from lower (or higher) layers to higher (or lower) layers with higher (or lower) concentrations of ozone, leading to lower (or increased) ozone concentrations at higher (or lower) layers. The warming of the Indian Ocean SST in the summer following El Niño enhances the SAH through two-level thermal adaptation, leading to ozone anomalies at lower latitudes in the ozone-valley region.

(3) The simulation-experiment results using the WACCM4 model were basically consistent with the observation results. The simulation results better reflect the influence of ENSO because the observation data contain other signals in addition ENSO.

Through this study, we can further understand the effect of ENSO on the ozone valley over the Tibetan Plateau and provide additional information on ozone formation.

Author Contributions: The central idea was mainly provided by Y.L., S.C., P.C. and D.G., Y.L. and S.C. analyzed the data and analyzed the results. L.W. conducted the simulation experiments. Y.L. prepared the figures. Y.L. and S.C. wrote the paper. D.G., S.C., F.X. and C.Y. contributed to refinement of the ideas and carried out additional analyses. All authors have read and agreed to the published version of the manuscript.

Funding: This research was funded by the National Key Research and Development Plan (2022YFF0801703), the National Natural Science Foundation of China (42005063, 42130604, and 41875048), the Integration Project of the National Natural Science Foundation of China Major Research Program (91837311), the Major Projects of the National Natural Science Foundation of China (42192512), the Program for Scientific Research Start-Up Funds of Guangdong Ocean University (060302032107), the Guangdong Provincial College Innovation Team Project (2019KCXTF021) and the First-Class Discipline Plan of Guangdong Province (080503032101 and 231420003).

Data Availability Statement: The ERA5 datasets in this study can be found at the https://cds.climate.copernicus.eu/ (accessed on 13 January 2023). To find out more about MERRA2 datasets, please visit https://disc.gsfc.nasa.gov/datasets/M2IMNPASM_5.12.4/ (accessed on 13 January 2023).

Acknowledgments: The authors would like to thank the editors and the reviewers for their valuable suggestions. We thank Chunhua Shi from the Nanjing University of Information Science and Technology for helpful discussions on the results.

Conflicts of Interest: The authors declare no conflict of interest.

References

1. de F. Forster, P.M.; Shine, K.P. Radiative forcing and temperature trends from stratospheric ozone changes. *J. Geophys. Res. Atmos.* **1997**, *102*, 10841–10855.
2. Haigh, J.D. The role of stratospheric ozone in modulating the solar radiative forcing of climate. *Nature* **1994**, *370*, 544–546. [CrossRef]
3. Kidston, J.; Scaife, A.A.; Hardiman, S.C.; Mitchell, D.M.; Butchart, N.; Baldwin, M.P.; Gray, L.J. Stratospheric influence on tropospheric jet streams, storm tracks and surface weather. *Nat. Geosci.* **2015**, *8*, 433–440. [CrossRef]
4. Randel, W.J.; Cobb, J.B. Coherent variations of monthly mean total ozone and lower stratospheric temperature. *J. Geophys. Res. Atmos.* **1994**, *99*, 5433–5447. [CrossRef]
5. Xie, F.; Tian, W.; Chipperfield, M.P. Radiative effect of ozone change on stratosphere-troposphere exchange. *J. Geophys. Res. Atmos.* **2008**, *113*, D00B09. [CrossRef]
6. Andrews, D.G.; Holton, J.R.; Leovy, C.B. *Middle Atmosphere Dynamics*; Academic Press: Cambridge, MA, USA, 1987.
7. Xia, Y.; Hu, Y.; Huang, Y.; Bian, J.; Zhao, C. Stratospheric ozone loss-induced cloud effects lead to less surface ultraviolet radiation over the Siberian Arctic in spring. *Environ. Res. Lett.* **2021**, *16*, 084057. [CrossRef]
8. He, Y.; Zhu, X.; Sheng, Z.; He, M.; Feng, Y. Observations of Inertia Gravity Waves in the Western Pacific and Their Characteristic in the 2015/2016 Quasi-biennial Oscillation Disruption. *J. Geophys. Res. Atmos.* **2022**, *127*, e2022JD037208. [CrossRef]
9. Ji, Q.; Zhu, X.; Sheng, Z.; Tian, T. Spectral Analysis of Gravity Waves in the Martian Thermosphere during Low Solar Activity Based on MAVEN/NGIMS Observations. *Astrophys. J.* **2022**, *938*, 97. [CrossRef]
10. Zhang, J.; Ji, Q.; Sheng, Z.; He, M.; He, Y.; Zuo, X.; He, Z.; Qin, Z.; Wu, G. Observation based climatology Martian atmospheric waves perturbation Datasets. *Sci. Data* **2023**, *10*, 4. [CrossRef]
11. Yu, Y.; Liu, B.; Ren, R.; Guan, Z.; Yang, Q.; Hu, M. Precursory Signals in the Stratospheric Meridional Mass Circulation for Mid-Latitude Cold Air Outbreak Events of High and Low Sub-Seasonal Predictability. *J. Geophys. Res. Atmos.* **2022**, *127*, e2022JD036814. [CrossRef]
12. He, Y.; Zhu, X.; Sheng, Z.; Ge, W.; Zhao, X.; He, M. Atmospheric Disturbance Characteristics in the Lower-middle Stratosphere Inferred from Observations by the Round-Trip Intelligent Sounding System (RTISS) in China. *Adv. Atmos. Sci.* **2022**, *39*, 131–144. [CrossRef]
13. He, Y.; Zhu, X.; Sheng, Z.; Zhang, J.; Zhou, L.; He, M. Statistical Characteristics of Inertial Gravity Waves Over a Tropical Station in the Western Pacific Based on High-Resolution GPS Radiosonde Soundings. *J. Geophys. Res. Atmos.* **2021**, *126*, e2021JD034719. [CrossRef]
14. Shi, C.; Zhu, J.; Cai, W. Characteristics and mechanism of troposphere-to-stratosphere transport dominated by a mesoscale convective complex in Southwest China. *Trans. Atmos. Sci.* **2022**, *45*, 302–311. [CrossRef]
15. Zhu, J.; Jin, X.; Shi, C.; Chen, D. The Troposphere-to-Stratosphere Transport Caused by a Rossby Wave Breaking Event over the Tibetan Plateau in Mid-March 2006. *Remote Sens.* **2023**, *15*, 155. [CrossRef]
16. Randel, W.J.; Polvani, L.; Wu, F.; Kinnison, D.E.; Zou, C.Z.; Mears, C. Troposphere-stratosphere temperature trends derived from satellite data compared with ensemble simulations from WACCM. *J. Geophys. Res. Atmos.* **2017**, *122*, 9651–9667. [CrossRef]
17. Xia, Y.; Huang, Y.; Hu, Y. On the climate impacts of upper tropospheric and lower stratospheric ozone. *J. Geophys. Res. Atmos.* **2018**, *123*, 730–739. [CrossRef]
18. Zhang, J.; Tian, W.; Xie, F.; Sang, W.; Guo, D.; Chipperfield, M.; Feng, W.; Hu, D. Zonally asymmetric trends of winter total column ozone in the northern middle latitudes. *Clim. Dyn.* **2019**, *52*, 4483–4500. [CrossRef]
19. Monforte, P.; Ragusa, M.A. Temperature trend analysis and investigation on a case of variability climate. *Mathematics* **2022**, *10*, 2202. [CrossRef]
20. Valipour, M.; Bateni, S.M.; Jun, C. Global surface temperature: A new insight. *Climate* **2021**, *9*, 81. [CrossRef]
21. Alexander, M.A.; Bladé, I.; Newman, M.; Lanzante, J.R.; Lau, N.-C.; Scott, J.D. The atmospheric bridge: The influence of ENSO teleconnections on air–sea interaction over the global oceans. *J. Clim.* **2002**, *15*, 2205–2231. [CrossRef]
22. Hu, J.; Li, T.; Xu, H.; Yang, S. Lessened response of boreal winter stratospheric polar vortex to El Niño in recent decades. *Clim. Dyn.* **2017**, *49*, 1–16. [CrossRef]
23. Xie, F.; Li, J.; Tian, W.; Zhang, J.; Shu, J. The impacts of two types of El Niño on global ozone variations in the last three decades. *Adv. Atmos. Sci.* **2014**, *31*, 1113–1126. [CrossRef]
24. Randel, W.J.; Garcia, R.R.; Calvo, N.; Marsh, D. ENSO influence on zonal mean temperature and ozone in the tropical lower stratosphere. *Geophys. Res. Lett.* **2009**, *36*, L15822. [CrossRef]
25. Zerefos, C.S.; Bais, A.F.; Ziomas, I.C.; Bojkov, R.D. On the relative importance of quasi-biennial oscillation and El Nino/Southern Oscillation in the revised Dobson total ozone records. *J. Geophys. Res. Atmos.* **1992**, *97*, 10135–10144. [CrossRef]

26. Langford, A.; Proffitt, M.; VanZandt, T.; Lamarque, J.F. Modulation of tropospheric ozone by a propagating gravity wave. *J. Geophys. Res. Atmos.* **1996**, *101*, 26605–26613. [CrossRef]
27. Zhou, R.; Cai, H.; Yi, M.; Guo, J. The impact of the ENSO cycle on the stratospheric aerosol distribution. *Chin. J. Geophys.* **2011**, *54*, 2726–2734. [CrossRef]
28. Benito-Barca, S.; Calvo, N.; Abalos, M. Driving mechanisms for the ENSO impact on stratospheric ozone. *Atmos. Chem. Phys. Discuss.* **2022**, *22*, 15729–15745. [CrossRef]
29. Gamelin, B.L.; Carvalho, L.; Kayano, M. The combined influence of ENSO and PDO on the spring UTLS ozone variability in South America. *Clim. Dyn.* **2020**, *55*, 1539–1562. [CrossRef]
30. Xie, F.; Zhang, J.; Li, X.; Li, J.; Wang, T.; Xu, M. Independent and joint influences of eastern Pacific El Niño–southern oscillation and quasi-biennial oscillation on Northern Hemispheric stratospheric ozone. *Int. J. Climatol.* **2020**, *40*, 5289–5307. [CrossRef]
31. Zhang, J.; Tian, W.; Wang, Z.; Xie, F.; Wang, F. The influence of ENSO on northern midlatitude ozone during the winter to spring transition. *J. Clim.* **2015**, *28*, 4774–4793. [CrossRef]
32. Zhou, X.; Luo, C.; Li, W.; Shi, J. Variation of total ozone over China and low value center over Qinghai-Tibet Plateau. *Chin. Sci. Bull.* **1995**, *15*, 1396–1398.
33. Bian, J.; King, G.; Chen, H.; Qi, D.; Lu, D.; Zhou, X. The tiny ozone hole appeared over the Tibetan Plateau in December 2003. *Chin. Sci. Bull.* **2006**, *51*, 606–609.
34. Guo, D.; Zhou, X.; Liu, Y.; Li, W.; Wang, P. The dynamic effects of the South Asian high on the ozone valley over the Tibetan Plateau. *Acta Meteorol. Sin.* **2012**, *70*, 1302–1311. [CrossRef]
35. Bian, J.; Yan, R.; Chen, H.; Lü, D.; Massie, S.T. Formation of the summertime ozone valley over the Tibetan Plateau: The Asian summer monsoon and air column variations. *Adv. Atmos. Sci.* **2011**, *28*, 1318–1325. [CrossRef]
36. Guo, D.; Su, Y.; Zhou, X.; Xu, J.; Shi, C.; Liu, Y.; Li, W.; Li, Z. Evaluation of the trend uncertainty in summer ozone valley over the Tibetan Plateau in three reanalysis datasets. *J. Meteorol. Res.* **2017**, *31*, 431–437. [CrossRef]
37. Liu, Y.; Li, W.; Zhou, X.; He, J. Mechanism of formation of the ozone valley over the Tibetan Plateau in summer—Transport and chemical process of ozone. *Adv. Atmos. Sci.* **2003**, *20*, 103–109. [CrossRef]
38. Liu, Y.; Li, W.; Zhou, X. A possible effect of heterogeneous reactions on the formation of the ozone valley over the Tibetan Plateau. *Acta Meteorol. Sin.* **2010**, *68*, 836–846.
39. Li, Y.; Chipperfield, M.P.; Feng, W.; Dhomse, S.S.; Pope, R.J.; Li, F.; Guo, D. Analysis and attribution of total column ozone changes over the Tibetan Plateau during 1979–2017. *Atmos. Chem. Phys.* **2020**, *20*, 8627–8639. [CrossRef]
40. Han, Z.; Chongping, J.; Libo, Z.; Wei, W.; Yongxiao, J. ENSO signal in total ozone over Tibet. *Adv. Atmos. Sci.* **2001**, *18*, 231–238. [CrossRef]
41. Zhang, J.; Tian, W.; Xie, F.; Li, Y.; Wang, F.; Huang, J.; Tian, H. Influence of the El Niño Southern Oscillation on the total ozone column and clear-sky ultraviolet radiation over China. *Atmos. Sci.* **2015**, *120*, 205–216. [CrossRef]
42. Wang, M.; Guo, S. lmpact of the ENSO cycle on the stratospheric ozone distribution over east Asia. *Plateau Meteorol.* **2017**, *36*, 865–874.
43. Roy, C.; Fadnavis, S.; Sabin, T. The stratospheric ozone rich cold intrusion during El-Niño over the Indian region: Implication during the Indian summer monsoon. *Int. J. Climatol.* **2021**, *41*, E233–E248. [CrossRef]
44. Chang, S.; Shi, C.; Guo, D.; Xu, J. Attribution of the Principal Components of the Summertime Ozone Valley in the Upper Troposphere and Lower Stratosphere. *Front. Earth Sci.* **2021**, 721. [CrossRef]
45. Xie, F.; Tian, W.; Zhou, X.; Zhang, J.; Xia, Y.; Lu, J. Increase in Lower Stratospheric Water Vapor in the Past 100 Years Related to Tropical Atlantic Warming. *Geophys. Res. Lett.* **2020**, *47*, e2020GL090539. [CrossRef]
46. Wang, W.; Hong, J.; Shangguan, M.; Wang, H.; Jiang, W.; Zhao, S. Zonally asymmetric influences of the quasi-biennial oscillation on stratospheric ozone. *Atmos. Chem. Phys.* **2022**, *22*, 13695–13711. [CrossRef]
47. Garcia, R.; Marsh, D.; Kinnison, D.; Boville, B.; Sassi, F. Simulation of secular trends in the middle atmosphere, 1950–2003. *J. Geophys. Res. Atmos.* **2007**, *112*, D09301. [CrossRef]
48. Marsh, D.R.; Mills, M.J.; Kinnison, D.E.; Lamarque, J.-F.; Calvo, N.; Polvani, L.M. Climate change from 1850 to 2005 simulated in CESM1 (WACCM). *J. Clim.* **2013**, *26*, 7372–7391. [CrossRef]
49. Chang, S.; Li, Y.; Shi, C.; Guo, D. Combined Effects of the ENSO and the QBO on the Ozone Valley over the Tibetan Plateau. *Remote Sens.* **2022**, *14*, 4935. [CrossRef]
50. Zhou, R.; Chen, Y. Ozone variations over the tibetan and lranian plateaus and their relationship with the south asia high. *J. Univ. Sci. Technol. China* **2005**, *35*, 899–908.
51. Wu, G.; Liu, p.; Liu, Y.; Li, W. Impacts of the sea surface temperature anomaly in theindian ocean on the subtropical anticycloneover the western pacific—Two-stage thermal adaptation in the atmosphere. *Acta Meteorol. Sin.* **2000**, *58*, 513–522.